Journal of the Optical Society of America A
OPTICS, IMAGE SCIENCE, AND VISION

Controlling electromagnetic scattering with wire metamaterial resonators

DMITRY S. FILONOV,[1,2,*] ALEXANDER S. SHALIN,[1] IVAN IORSH,[1] PAVEL A. BELOV,[1] AND PAVEL GINZBURG[2]

[1]ITMO University, St. Petersburg 197101, Russia
[2]School of Electrical Engineering, Tel Aviv University, Tel Aviv 69978, Israel
*Corresponding author: dmitriif@mail.tau.ac.il

Received 13 May 2016; revised 14 August 2016; accepted 14 August 2016; posted 16 August 2016 (Doc. ID 265215); published 2 September 2016

Manipulation of radiation is required for enabling a span of electromagnetic applications. Since properties of antennas and scatterers are very sensitive to the surrounding environment, macroscopic artificially created materials are good candidates for shaping their characteristics. In particular, metamaterials enable controlling both dispersion and density of electromagnetic states, available for scattering from an object. As a result, properly designed electromagnetic environments could govern wave phenomena and tailor various characteristics. Here electromagnetic properties of scattering dipoles, situated inside a wire medium (metamaterial), are analyzed both numerically and experimentally. The effect of the metamaterial geometry, dipole arrangement inside the medium, and frequency of the incident radiation on the scattering phenomena is studied in detail. It is shown that the resonance of the dipole hybridizes with Fabry–Perot modes of the metamaterial, giving rise to a complete reshaping of electromagnetic properties. Regimes of controlled scattering suppression and super-scattering are experimentally observed. Numerical analysis is in agreement with the experiment, performed at the GHz spectral range. The reported approach to scattering control with metamaterials could be directly mapped into optical and infrared spectral ranges by employing scalability properties of Maxwell's equations.

OCIS codes: (290.0290) Scattering; (120.5820) Scattering measurements; (160.3918) Metamaterials.

http://dx.doi.org/10.1364/JOSAA.33.001910

1. INTRODUCTION

Radiation and scattering properties of either optical emitters or classical antennas, embedded in a medium, could be substantially different from those of isolated structures. These effects are quite commonly observed with radio waves, where couplings, cross talks, and other concomitant effects should be taken into account for a complete analysis or engineering of certain characteristics. For example, the performance of directional antennas relies on careful design of the interference between a feeding element and a collection of resonant scatterers (impedance matching) [1]. Similar effects in the optical domain are usually treated via the photonic density of states concept; here the spontaneous emission rate enhancement with a photonic cavity is referred to as the Purcell effect [2]. However, radiation efficiencies at any spectral range could be described with a unified mathematical approach, based on classical electromagnetic Green's functions [1]. From the classical point of view, this result is the direct consequence of the Maxwell's equations scalability in respect to an operation frequency. Remarkably, quantum dynamics of emission processes in both weak and strong coupling regimes could be analyzed with the help of classical electromagnetic Green's functions, as a result of the fundamental causality and fluctuation-dissipation relations [3]. This classical–quantum correspondence enables experimental investigation and emulation of complex photonic processes with lower frequencies, where both fabrication and measurements are routinely available. However, the distinctive discrepancy between electromagnetic phenomena at different frequencies is the lack of scalability in material parameters, since complex permittivities and permeabilities are frequency-dependent. These properties, being predetermined by nature, could, however, be modified by subwavelength structuring. This concept of metamaterials (e.g., [4,5]) has been successfully employed for obtaining intriguing material properties, such as negative ϵ and μ [6], with following demonstrations of invisibility cloaking [7] and other remarkable phenomena. The impact of structured environment on radiation properties of quantum emitters gained additional attention with the introduction of the concept of "hyperbolic metamaterials" [8]. The key property of hyperbolic media is to deliver extremely high and broadband Purcell factors, virtually limited by the granularity of the structures' realization [9]. An additional feature of this macroscopic type of enhancement is its relative insensitivity to the emitter's position within the structure, which is in direct

contrast to the antenna approach, relying on localized fields and interference phenomena [10,11].

While the metamaterials' impact on radiation efficiencies is widely studied, their ability to manipulate electromagnetic scattering properties of embedded objects is less explored. Nevertheless, these phenomena are tightly related. Both could be described with either the density of electromagnetic states concept or by utilizing the electromagnetic Green's functions approach. However, elastic (e.g., electromagnetic scattering) versus inelastic (e.g., Compton scattering [12]) aspects of interactions should be properly addressed. As an additional example, the discrete diffraction phenomenon in waveguide arrays [13] utilizes a controllably reduced number of electromagnetic modes, available for an interaction. Metamaterials exploit a similar approach of configuring the spatial dependence of modes with additional remarkable flexibility of controlling their density of states.

Here, comprehensive numerical and experimental investigations of electromagnetic scattering from dipoles, embedded in a finite-size wire medium, are reported. Scattering properties were investigated by varying the dipoles' lengths (90–110 mm), their spatial arrangements, and incident radiation frequencies (in the range of 0.2–2 GHz). Special attention was paid to whether dipoles have direct electrical contact with the wires forming the metamaterial (Fig. 1). The performed analysis paves the way for addressing a variety of fundamental light–matter interaction phenomena by means of emulation experiments, as will be discussed hereafter.

2. RESULTS

A medium composed of parallelly aligned perfectly conducting wires has many remarkable electromagnetic properties [14]. These densely packed wires prohibit the propagation of electromagnetic waves polarized along their principal direction and support TEM types of modes (both electric and magnetic fields are perpendicular to the propagation direction). This phenomenon results in degenerately flat dispersion diagrams while the subwavelength (yet finite) periodicity leads to inherently strong spatial dispersion [15]. The field distributions of modes supported by the structure are substantially different from those of the free space and have remarkable properties that could be employed for various applications, e.g., imaging beyond the classical (free space) diffraction limit (see, e.g., [16]). It is worth noting that the optical counterpart of a densely packed nanorods array could support elliptical, hyperbolic, and compound (nonlocal) dispersion regimes, depending on the frequency [17,18]. This phenomenon could be also employed for subdiffraction "hyperlensing" [19] and other applications. In all the above cases (optical and microwave), the density and spatial distribution of electromagnetic modes are substantially different from those of free space, and as a result, a severe impact on the scattering processes and diffraction is expected. These effects will be underlined during the discussion of the results presented in the following sections.

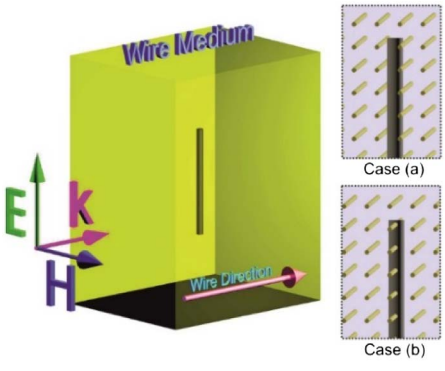

Fig. 1. Schematics of the considered structure: finite size metamaterial (wire medium) with an embedded scatterer (a dipole). Two interaction scenarios are considered: (a) noncontact mode, where the dipole is not touching the wires, and (b) contact mode, where the dipole is touching the wires.

A. Dipoles in a Wire Medium—A Noncontact Mode

In order to obtain efficient scattering from a perfectly conducting object, the physical dimensions of the latter should be comparable with the wavelength of the excitation. It is worth noting that in the optical domain subwavelength, objects could have enormously large scattering cross sections by exploiting the localized plasmon resonance phenomenon [20,21]. Scattering from thin metal wires in the microwave regime has the first resonance when the object's length along the polarization direction of the incident wave reaches the half-wavelength scale. Hereafter, dipolar antennas (called dipoles here) with lengths of 90, 100, and 110 mm and diameters of 7.5 mm will be considered. Total scattering (radar) cross sections (RCSs) of the dipoles in free space appear in Fig. 2(a), where different color lines correspond to three different dipole lengths. All the numerical

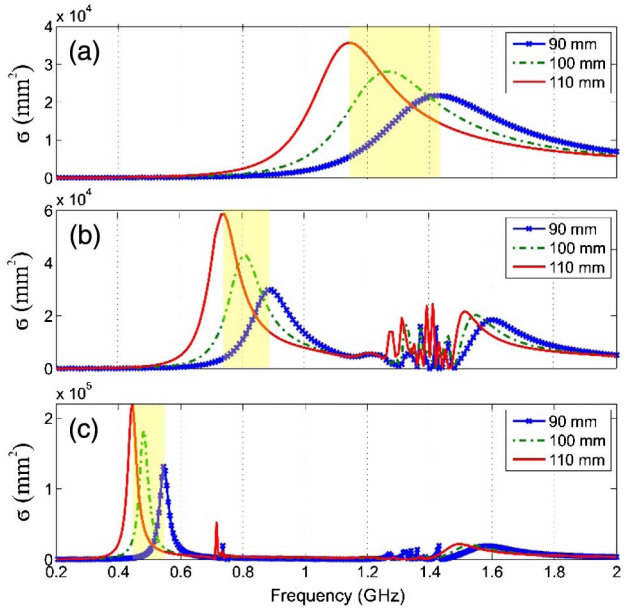

Fig. 2. Scattering/radar cross sections of dipoles (a) in free space, (b) in wire medium, noncontact mode, and (c) in wire medium, contact mode. Solid blue with dots, dash-dotted green, and solid red lines correspond to the dipole lengths of 90, 100, and 110 mm, respectively. The metamaterial consists of 16 × 26 (scatterer does not intersect with the wires) and 17 × 26 (scatterer intersects with the wires) thin metal wires, with 2 mm diameter, 200 mm length, and 10 mm period. Shaded regions on all the panels indicate the bandwidth of the main peak shift with variation of the wire's length.

results were obtained with the help of the finite element method [22]. (Additional information appears in Section 2.F.) Next, the half-wavelength (at different frequencies) dipoles were situated inside the wire medium *without* having direct electrical contact with the surrounding structure [Fig. 1(a)]. The metamaterial consists of a 16 × 26 array of thin 200 mm long metal wires, with diameters of 2 mm and a period of 10 mm. The dipole orientation is perpendicular to the direction of the wires, as appears in the insets to Fig. 1. The resulting RCSs appear in Fig. 2(b). The RCSs of dipoles in the wire medium are red shifted with respect to the free space scenario, and peaks fall within the range of 0.7–1 GHz (major contribution of the wires). Furthermore, the set of blue-shifted resonances (1.5–1.8 GHz) and the collection of fast-oscillating features appear in the spectra. The latter results from the contribution of the higher order modes of the finite size wires array and will be the subject of a future investigation. The main focus will be made on the strong interaction between the scatterer and the low-order modes of the metamaterial structure.

Since the dipole scatterer is situated at the point of high symmetry of the metamaterial (at the center), it could couple only to the high symmetry (even) modes. The major RCS peak corresponds to the lowest even mode, while the second one (at the higher frequency) is a signature of the interaction with the second symmetric mode. For the extended frequency range, the signatures of higher order modes will be observed. Since the excitation of the odd modes is symmetry forbidden, there is a scattering suppression at the entire gap in between two major RCS peaks. This type of scattering suppression in the vicinity of the super-scattering spectral window is quite common. For example, consideration of fundamental causality and energy conservation principles in analysis of frequency-dependent scattering properties leads to an appearance of strong extinction peaks in the spectral vicinity of suppressed areas due to the existence of causality relations [23], unless diamagnetic materials are involved [24]. The spectral positions of the RCS peaks on Fig. 2(b) could be tailored by varying the parameters of the metamaterial, specifically the wire length.

Figure 3(a) shows the RCS dependence for the set of six wire lengths (50–300 mm) in the case of noncontact mode (scattering dipole not touching the wires), while the dipole's dimensions are kept the same (110 mm). The increase of the length shifts the first Fabry–Perot resonance to lower frequencies, as can be seen in Fig. 3(a). Similar behavior takes place in classical Fabry–Perot etalons, where an increase of the bulk material thickness leads to the red shift of the first fundamental resonance. The behavior of the second even mode is similar: It replicates the trends of the main one. It should be noted, however, that the shifts do scale linearly with the wires length, but the proportionality coefficient is not unity, as might be expected from a simple resonator theory. A nontrivial scaling factor in finite size metamaterial cavities results from both modal dispersion inside the metamaterial and two other transversal dimensions that were kept constant in the studies here [25].

B. Dipoles in a Wire Medium—Contact Mode

In the next set of investigations, the dipole scatterer was placed in direct contact with the wires. In order to preserve the

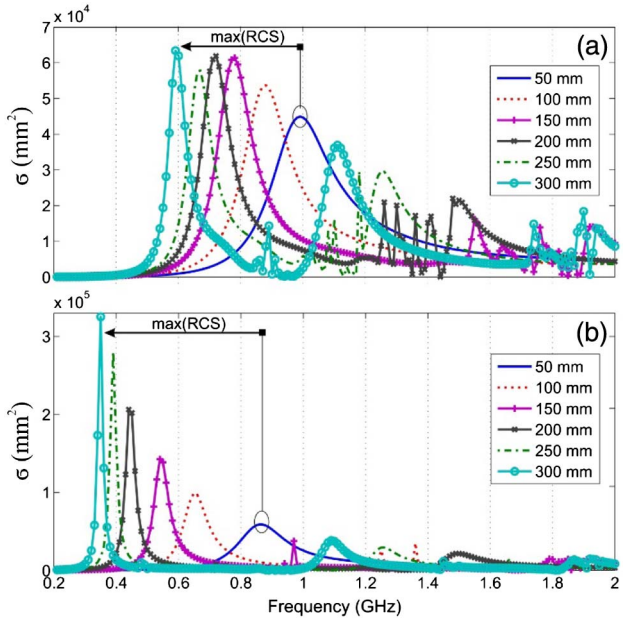

Fig. 3. Scattering/radar cross sections of 110 mm dipole in metamaterial resonators with four different lengths of constituting wires: (a) noncontact mode and (b) contact mode. The length of the wires changes from 50 to 300 mm (from blue to cyan) in steps of 50 mm. Other parameters of the structure are the same as the ones used for Fig. 2.

symmetry of the structure, the metamaterial consists of 17 × 26 wires. (The dipole touches the ninth wire.) The introduction of this electrical contact changes the nature of the coupling phenomenon from capacitive (noncontact mode) to conducting. The metamaterial's rods are now shorted in their middles, enabling the free flow of current between a few of the connected wires. The RCSs for three different dipoles intersecting the middle row of metamaterial wires are shown in Fig. 2(c). The distinctive difference between these results and the noncontact case is the stronger red shift of the main resonance and its narrowing. The red shift results from effectively elongating the wire. Moreover, the u-band shape of shortened conductors leads to concave geometry, which is also responsible for the red shift [26]. It should be mentioned that in the contact case the field is more localized within the wire medium, which is the reason for the Q-factor increase and the corresponding resonances narrowing. The fields' structure will be discussed in detail in the next section. The RCS peaks are strongly dependent on the length of the wires, constituting the metamaterial, similar to the noncontact case. Figure 3(b) shows the structure of scattering peaks for different geometries. A much more pronounced and broadband scattering suppression window is observed in the contact mode case, compared to the noncontact scenario. The main reason for this occurrence is the suppressed current on the dipolar scatterer, as it is physically separated to a collection of small sections, each one shortened by the metamaterial's wires. (This shortage is a resonant effect, as will be shown hereafter.) A distinctive difference between contact and noncontact modes originates from allowing/disallowing the current flow along the scattering dipole. This intuitive

description will be supported by numerical results, presented in the next section.

Similar phenomena occur in optics, where capacitive or conductive coupling between nontouching/touching noble metal particles controls the spectral response of localized plasmon resonances [26]. Moreover, the narrowing of the resonance (quality factor increase) is also an attribute of plasmonic resonances [26]. The difference between optical and GHz spectral ranges lies in the nature of the involved electromagnetic currents. In optics, polarization currents should be considered instead of the conduction ones at lower frequencies.

C. Electromagnetic Fields Inside the Wire Medium

The structure of the electromagnetic fields inside the metamaterial resonator will be investigated next in order to verify behaviors at scattering suppression and super-scattering regions. Figures 4(a)–4(d) show the intensity distribution of electric fields in the systems, considered in Fig. 3. Figure 4(a) shows the field intensity at the frequency of 1.12 GHz, where the RCS of the 110 mm dipole has a maximum in the free space as shown in Fig. 2(a), while the plots for noncontact and contact configurations at the same illumination frequency appear in Figs. 4(b) and 4(d), respectively. Cross sections are given for the back facet ($x = 0$), the middle plane including the dipole ($y = 0$), and the bottom side ($z = 100$ mm) of the metamaterial block. Figures 4(c) and 4(e) correspond to the frequency of the major RCS maxima, affected by the metamaterial—noncontact and contact modes, respectively. Frequencies of the maxima are 0.74 and 0.445 GHz.

The scattering suppression is observed for both noncontact and contact cases, as could be observed from both RCS values in Figs. 2(b) and 2(c) and the field distributions in Figs. 4(b) and 4(d). While in both cases flat wavefronts are relatively undistorted by the dipolar scatterer, the contact case delivers better scattering suppression, as the effective shortage of the dipole with wires, composing the metamaterial, strongly affects the current flow along the dipole, and the metamaterial wires are also weakly polarized (the whole structure has smaller RCS). Regimes of strong and suppressed scattering could also be verified by observing surface currents, flowing on the dipole. Currents were derived numerically for each one of the scattering scenarios on Fig. 4 and are represented on the corresponding panels [Figs. 4(f)–4(j)]. It is worth underlining that the different color map values were chosen for a better visibility, while the maximal values of surface current are indicated explicitly on each panel (the amplitude of the incident field was chosen to be 1 V/m). All the cases should be compared with the free space scenario [Fig. 4(f)]. First, the values of the current in the strong scattering regimes are much higher than in the case of the standalone dipole (factor of 1.7 in the noncontact and 5.5 in the contact regimes). Those values, however, cannot be directly compared with RCS peaks ratios (Fig. 2), as the incident field frequencies are different and the wire media affects the effective impedance of the whole radiating structures. Second, in the scattering suppression case, the wires reduce the current by factors of 5 (noncontact) and 1.1 (contact). The remark from the previous sentence also applies in this case. The current on the dipole in all of the cases is nearly sinusoidal.

It is worth noting that the RCS of the metamaterial block without the scatterer is very small. It was estimated to be as small as 0.25% of its physical cross section. This result should not come as a surprise, since the polarization of the wave is perpendicular to the wire direction. The physical dimension of an individual wire in the plane of polarization is 2 mm, which is small compared with the wavelength of the incident wave ($2/150 \ll 1$).

Strong interaction between the dipolar scatterer and the metamaterial causes the reshaping of the RCS structure. In particular, as was already mentioned above, the major RCS peaks are red shifted. The fields at those new RCS maxima

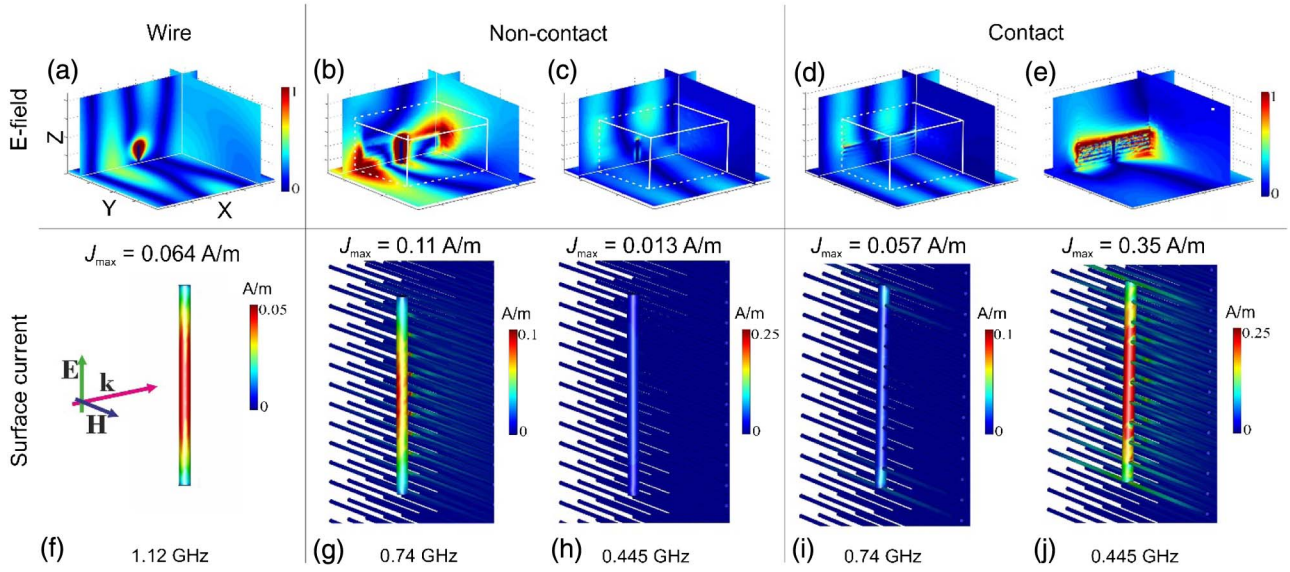

Fig. 4. Field intensity maps [(a), (b), and (d) 1.12 GHz; (c) 0.74 GHz; (e) 0.445 GHz]. (a) Dipole in a free space. (b) and (c) Noncontact mode. (d) and (e) Contact mode. The structure is excited with a plane wave (intensity equal to unity), propagating from the left to the right (upper left panel). Other parameters of the structure are the same as those used for Fig. 2.

appear in Figs. 4(c) and 4(e). The fields at 0.74 GHz in the noncontact mode are strongly enhanced by the entire structure, which collectively resonates with the incident field. A well-defined field maximum is obtained in the location of the dipole, the impedance of which is better matched to the free space with the help of metamaterial resonator. On the other side, in the contact mode at 0.445 GHz, the field on the dipole vanishes due to the beforehand mentioned shortage. The main contribution to the radiation is delivered now by the metamaterial. As could be seen, metamaterial wires act as a collection of antennas, reradiating the excitation. All those field behaviors are consistent with the far field signatures, obtained via RCS calculations (Fig. 2).

D. Dipoles, Displaced from the Center of the Wire Medium

The systems considered above have distinctive reflection symmetry. This symmetry prohibits the excitation of odd modes, which could emerge in the spectrum once the scatterer is displaced from the metamaterial's center. Figures 4(a) and 4(b) show the changes in spectra for noncontact and contact modes in cases where the scatterer has been shifted from the symmetry point. The appearance of odd modes could be clearly seen in both cases. As the modes have finite spectral width, they overlap and interfere with each other. This effect is pronounced for the noncontact case [Fig. 5(a)] and manifests itself in fast RCS oscillations in the vicinity of the major peak—0.7 GHz. In the contact case this effect is less important. Nevertheless the odd modes affect the scattering suppression region. The effective bandwidth of the frequency range of scattering suppression is reduced and odd mode peaks appear within the gap.

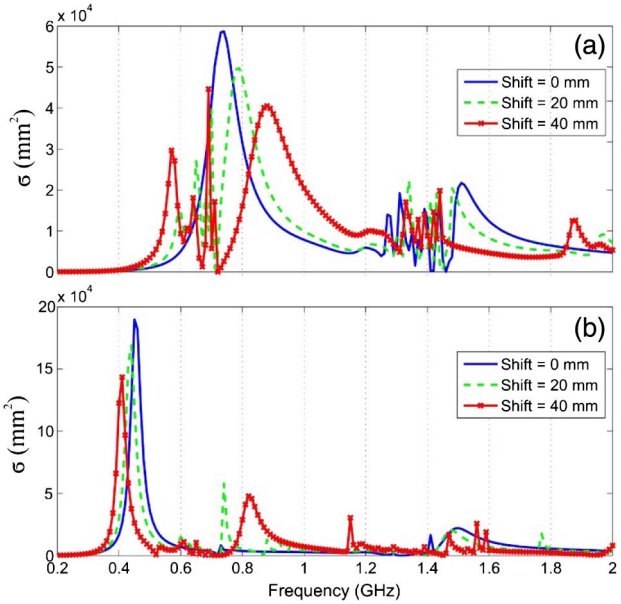

Fig. 5. Scattering/radar cross sections of a 110 mm dipole in the metamaterial, made of 200 mm length wires: (a) noncontact mode and (b) contact mode. Three curves on each panel correspond to the dipole position in respect to the structure's center. Plots corresponding to 0, 20, and 40 mm shifts are marked by solid blue, dashed green, and solid red with dots, respectively. The parameters of the wire medium are the same as those used for Fig. 2.

E. Experimental Observation of Scattering on a Dipole in the Noncontact Mode

In order to verify the numerical predictions, experimental studies were performed in an anechoic chamber. The measurements were conducted in the following manner: A rectangular horn antenna (TRIM 0.75 GHz to 18 GHz; DR) was connected to a transmitting port of the vector network analyzer Agilent E8362C. This configuration replicates a plane wave excitation with good accuracy. The wire medium was placed in the far-field region of the antenna, and the similar horn (TRIM 0.75 GHz to 18 GHz) was employed as a receiver (3.5 m is the distance between the horns). The medium consists of a 16 × 26 array of parallel brass wires (2 mm diameter and 200 mm length). The period of the structure along the X and Y directions is equal to 10 mm. The effective scattering cross sections were extracted from imaginary parts of the forward scattering amplitudes (according to the optical theorem) [27].

Experimentally obtained RCSs appear in Fig. 6. The black dotted line represents the dipole in free space, while the red solid line stands for the scattering inside the metamaterial (noncontact mode). Comparing the experiment with the numerical predictions [Figs. 2(a) and 2(b)] enables observing a good correspondence between the two. It should be noted, however, that the relative heights of RCS peaks, obtained with the simulation and experiment, do not agree. This effect is generally related to the complexity of the free space setup calibration over a wide range of frequencies. Furthermore, the sensitivity of the vector network analyzer drops fast with lowering frequency, making noise impact more severe. Additional undesired oscillatory behavior in the experimental scattering spectra corresponds to the set of artificial Fabry–Perot resonances between the wire medium interface as well as between the transmitting and receiving horn antennas. Additional discrepancies between the experimental and numerical results emerge mainly due to the wavelength-dependent wavefront distortions of the incident wave produced by the horn antenna, which quite commonly appear in lab experiments of this kind. Nevertheless, strong scattering suppression at a wide GHz spectral window, predicted by numerical analysis, was confirmed experimentally.

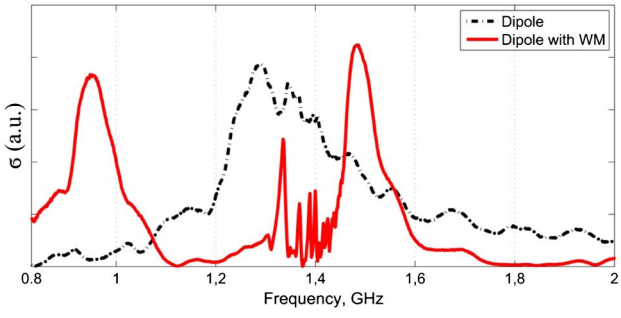

Fig. 6. Experimental scattering/radar cross sections (arb. units). Red solid line: 100 mm dipole in 200 mm metamaterial (noncontact mode); black dot-dashed line: the same dipole in free space. The parameters of the wire medium are the same as those used for Fig. 2.

F. Details of Numerical Method

All the numerical results were obtained with the help of the finite element method and subsequently verified with a time-domain solver [22]. Finite-size structures were placed in a large simulation domain (far field) with scattering boundary conditions imposed. Variable mesh with overall 250,000 cells was utilized and stability of solutions was checked. Plane wave excitation was generated by one port, located on the left facet of the simulation domain, while the collecting port was placed on the opposite side, enabled forward scattering calculation. The optical theorem was employed for calculating the total RCS.

3. DISCUSSION AND CONCLUSION

The scalability of physical laws (especially Maxwell's equations) in respect to a dimensionless parameter (in electrodynamics, wavelength over characteristic dimension of a system) is a very powerful tool. Scaling up the systems' physical dimensions makes their fabrication and measurements much more straightforward and gives numerous advantages for detailed investigation. By performing scattering experiments with microwaves in structured media we have advanced an emulation tool, enabling the investigation of complex light–matter interactions at the nanoscale. In particular, it is quite useful to consider a counterpart of emission/scattering resonance shifts taking place in the optical domain. Dynamically stimulated shifts of quantum energy levels is referred to as the AC Stark effect, while the shift due to the virtual photon exchange with the surrounding is referred to as the Lamb shift [28]. Observation of these effects is relatively complex, especially once auxiliary nanostructures are involved. However, in both cases (AC Stark and Lamb shifts) classical–quantum correspondence could be drawn and, as a result, all the information is encapsulated in the knowledge of the electromagnetic Green's function. For example, the Lamb shift is proportional to the real part of the Green's function [3]; nevertheless the virtual photon exchange cannot be mapped directly due to the strong thermal noise above the vacuum limit in the case of lower frequencies. However, in the optical domain the observation of those shifts is much more challenging than with radio waves, due to the naturally small dipolar moments. Nevertheless, general trends in optics could be predicted with RF modeling and experiments, underlining the significance of the emulation experiments. Furthermore, as was recently shown, relatively small (orders of tens) finite arrays of rods could predict the light–matter interaction behavior of infinitely large systems [25,29]. The experimental platform, discussed in Section 2.E, could be used for experimental verification of the above theoretical predictions.

As an additional aspect, the deep subwavelength nature of interactions, material granularity, and spatial dispersion could impact various types of newly proposed phenomena, e.g., self-induced torques [30] and cloaking [31] to name a few. Emulation experiments, similar to the one proposed here, could serve as auxiliary tools and enable further detailed investigations.

To summarize, numerical and experimental investigations of scattering from objects, embedded in a metamaterial assembly, were reported. In particular, tailoring electromagnetic properties of the embedding medium was demonstrated to provide a tool for significant shifting of the scattering resonant frequency due to a strong coupling between the scatterer and the metamaterial. Moreover, it has been shown that the direct electric contact between the scatterer and the embedding metamaterial dramatically changes the interaction nature, making it conductive instead of capacitive. Shortage between the wires causes an almost twice-stronger effect in terms of the resonance shift. For a brief comparison, controllable investigation of contact/noncontact regimes between closely situated complex nanostructures is a very challenging task, underlining the strength of the emulation approach. Metamaterials, the wire medium in particular, could create reduced space for modes that are available for wave diffraction and, as a result, manipulate scattering properties of embedded objects. Creation of reduced diffraction and controlled scattering regimes is beneficial for various applications, e.g., invisibility cloaking [32]. Detailed emulation experiments with microwaves pave a way for designing experiments in the optical domain.

Funding. Government of the Russian Federation (074-U01, SP-4248.2016.1); Ministry of Education and Science of the Russian Federation (GOSZADANIE 2014/190); Russian Foundation for Basic Research (RFBR) (16-52-00112); Tel Aviv University (TAU) Rector Grant; German-Israeli Foundation for Scientific Research and Development (GIF) (2399).

Acknowledgment. P. G. acknowledges the support from TAU Rector Grant and German-Israeli Foundation (GIF). A. S. acknowledges the support of the President of Russian Federation in the frame of Scholarship SP-4248.2016.1.

REFERENCES

1. C. A. Balanis, *Antenna Theory: Analysis and Design* (Wiley-Interscience, 2005).
2. E. M. Purcell, "Spontaneous emission probabilities at radio frequencies," Phys. Rev. **69**, 37–38 (1946).
3. W. Vogel and D.-G. Welsch, *Quantum Optics*, 3rd. (Wiley-VCH, 2006).
4. R. W. Z. Nader Engheta, *Metamaterials: Physics and Engineering Explorations* (Wiley-IEEE, 2006).
5. W. Cai and V. Shalaev, *Optical Metamaterials: Fundamentals and Applications* (Springer, 2010).
6. V. M. Shalaev, "Optical negative-index metamaterials," Nat. Photonics **1**, 41–48 (2007).
7. D. Schurig, J. J. Mock, B. J. Justice, S. A. Cummer, J. B. Pendry, A. F. Starr, and D. R. Smith, "Metamaterial electromagnetic cloak at microwave frequencies," Science **314**, 977–980 (2006).
8. Z. Jacob, I. I. Smolyaninov, and E. E. Narimanov, "Broadband Purcell effect: radiative decay engineering with metamaterials," Appl. Phys. Lett. **100**, 181105 (2012).
9. A. N. Poddubny, P. A. Belov, P. Ginzburg, A. V. Zayats, and Y. S. Kivshar, "Microscopic model of Purcell enhancement in hyperbolic metamaterials," Phys. Rev. B **86**, 035148 (2012).
10. L. Novotny and N. van Hulst, "Antennas for light," Nat. Photonics **5**, 83–90 (2011).
11. J.-J. Greffet, "Applied physics: nanoantennas for light emission," Science **308**, 1561–1563 (2005).
12. I. V. Iorsh, A. N. Poddubny, P. Ginzburg, P. A. Belov, and Y. S. Kivshar, "Compton-like polariton scattering in hyperbolic metamaterials," Phys. Rev. Lett. **114**, 185501 (2015).
13. D. N. Christodoulides, F. Lederer, and Y. Silberberg, "Discretizing light behaviour in linear and nonlinear waveguide lattices," Nature **424**, 817–823 (2003).

14. C. R. Simovski, P. A. Belov, A. V. Atrashchenko, and Y. S. Kivshar, "Wire metamaterials: physics and applications," Adv. Mater. **24**, 4229–4248 (2012).
15. P. A. Belov, R. Marqués, S. I. Maslovski, I. S. Nefedov, M. Silveirinha, C. R. Simovski, and S. A. Tretyakov, "Strong spatial dispersion in wire media in the very large wavelength limit," Phys. Rev. B **67**, 113103 (2003).
16. F. Lemoult, G. Lerosey, J. de Rosny, and M. Fink, "Resonant metalenses for breaking the diffraction barrier," Phys. Rev. Lett. **104**, 203901 (2010).
17. R. J. Pollard, A. Murphy, W. R. Hendren, P. R. Evans, R. Atkinson, G. A. Wurtz, A. V. Zayats, and V. A. Podolskiy, "Optical nonlocalities and additional waves in epsilon-near-zero metamaterials," Phys. Rev. Lett. **102**, 127405 (2009).
18. P. Ginzburg, F. J. Rodríguez Fortuño, G. A. Wurtz, W. Dickson, A. Murphy, F. Morgan, R. J. Pollard, I. Iorsh, A. Atrashchenko, P. A. Belov, Y. S. Kivshar, A. Nevet, G. Ankonina, M. Orenstein, and A. V. Zayats, "Manipulating polarization of light with ultrathin epsilon-near-zero metamaterials," Opt. Express **21**, 14907–14917 (2013).
19. Z. Jacob, L. V. Alekseyev, and E. Narimanov, "Optical hyperlens: far-field imaging beyond the diffraction limit," Opt. Express **14**, 8247–8256 (2006).
20. S. A. Maier, *Plasmonics: Fundamentals and Applications* (Springer, 2007).
21. N. Berkovitch, P. Ginzburg, and M. Orenstein, "Nano-plasmonic antennas in the near infrared regime," J. Phys. **24**, 073202 (2012).
22. "CST STUDIO SUITE," https://www.cst.com/products/csts2.
23. F. Monticone and A. Alù, "Do cloaked objects really scatter less?" Phys. Rev. X **3**, 041005 (2013).
24. F. Monticone and A. Alù, "Physical bounds on electromagnetic invisibility and the potential of superconducting cloaks," Photon. Nanostr. Fundam. Appl. **12**, 330–339 (2014).
25. A. P. Slobozhanyuk, P. Ginzburg, D. A. Powell, I. Iorsh, A. S. Shalin, P. Segovia, A. V. Krasavin, G. A. Wurtz, V. A. Podolskiy, P. A. Belov, and A. V. Zayats, "Purcell effect in hyperbolic metamaterial resonators," Phys. Rev. B **92**, 195127 (2015).
26. N. Berkovitch, P. Ginzburg, and M. Orenstein, "Concave plasmonic particles: broad-band geometrical tunability in the near-infrared," Nano Lett. **10**, 1405–1408 (2010).
27. D. R. H. Craig and F. Bohren, *Absorption and Scattering of Light by Small Particles* (Wiley-VCH, 1998).
28. R. Liboff, *Introductory Quantum Mechanics*, 4th ed. (Addison-Wesley, 2002).
29. M. S. Mirmoosa, S. Y. Kosulnikov, and C. R. Simovski, "Unbounded spatial spectrum of propagating waves in a polaritonic wire medium," Phys. Rev. B **92**, 075139 (2015).
30. P. Ginzburg, A. V. Krasavin, A. N. Poddubny, P. A. Belov, Y. S. Kivshar, and A. V. Zayats, "Self-induced torque in hyperbolic metamaterials," Phys. Rev. Lett. **111**, 036804 (2013).
31. A. S. Shalin, P. Ginzburg, A. A. Orlov, I. Iorsh, P. A. Belov, Y. S. Kivshar, and A. V. Zayats, "Scattering suppression from arbitrary objects in spatially dispersive layered metamaterials," Phys. Rev. B **91**, 125426 (2015).
32. P.-Y. Chen, J. Soric, and A. Alù, "Invisibility and cloaking based on scattering cancellation," Adv. Mater. **24**, OP281–OP304 (2012).